Electronic Supplementary Information for

All-boron planar ferromagnetic structures: from cluster to monolayer

Chang-Chun He,[a,b] Shao-Gang Xu,[b] Yu-Jun Zhao,[a] Hu Xu,*[b] and Xiao-Bao Yang*[a,c]

[a] Department of Physics, South China University of Technology, Guangzhou 510640, P.R. China
[b] Department of Physics & Institute for Quantum Science and Engineering and Guangdong Provincial Key Laboratory of Computational Science and Material Design, Southern University of Science and Technology, Shenzhen 518055, P. R. China
[c] Guangdong Provincial Key-lab for Computational Science, Shenzhen 518000, P. R. China
Corresponding author Email: xuh@sustc.edu.cn; scxbyang@scut.edu.cn

Calculation Parameters Test

The calculation parameters has been carefully tested to confirm the accuracy. Below we show the test of cutoff energy, where the cutoff energy of 480 eV (denoted by the red dot) is selected as the proper cutoff energy parameter. Similarly, K points is also tested, we selected the k-points spacing of 0.1 Å (denoted by the red dot) to be the proper parameter for the total energy calculations.

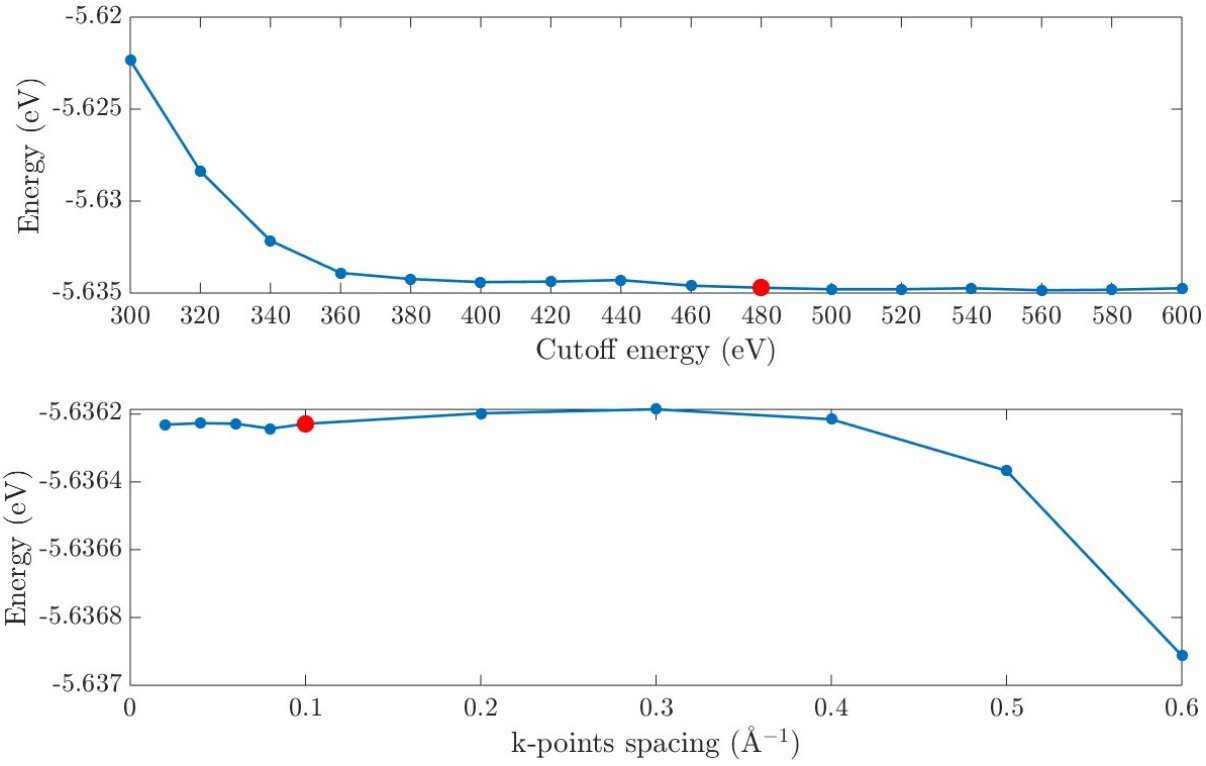

Figure S1. The energy coverage test for cutoff energy and k-points spacing.

In the HSE06 calculation, a smaller energy convergence criterion (10^{-6} eV), a larger energy cutoff (520 eV) and a denser *k-mesh* (0.05 k-points spacing) are employed to keep the accuracy. In addition, we set HFSCREEN = 0.2 .

Cohesive Energy Comparison

We refer to the review article from Guo's group[1], the experimental research from Wang's group[2] and the theoretical research from Zeng's group[3]. The planar boron clusters with the number between 30 and 40 are selected for the comparison of cohesive energy as listed in Table S1. All the calculations are carried out using the Perdew-Burke-Ernzerhof (PBE) functional. The cohesive energy E_c in boron clusters and monolayers is defined by $E_c = \left(nE_{isolated} - E_{total}\right)/n$ (E_{total} is the total energy of the boron structures, n is the number of the boron structures and $E_{isolated}$ is the energy of one isolated boron atom.)

Table S1. Calculated cohesive energy per atom of boron clusters.

Boron cluster	E_c (eV/atom)
B_{34} (S=1) (Fig. 2b)	5.538
B_{34} (S=2) (Fig. 2b)	5.542
B_{34} (S=3) (Fig. 2b)	5.537
B_{52} (S=4) (Fig. 2b)	5.531
B_{30} (point group: C_1)[1]	5.586
B_{30} (point group: C_{6v})[1]	5.349
B_{34} (points group: C_1)[2]	5.617
B_{35} (point group: C_s)[1]	5.618
B_{36} (point group: C_{6v})[1]	5.674

Although the freestanding magnetic boron clusters are not energetically favorable than the boron clusters which are confirmed in previous theoretical and experimental works, it is shown that these magnetic boron clusters may be synthesized more easily on metal substrates according to our calculations as shown in Fig. S1. We have calculated the cohesive energy of these predicted clusters on Cu(111), Au(111), Ag(111) substrates which are suitable metal substrate for the growth of boron clusters. The cohesive energy is defined by

$$E_c = \left(E_{substrate} + E_{cluster} - E_{total}\right)/n,$$

where $E_{total}, E_{substrate}, E_{cluster}$ are the total energy of the boron cluster in metal substrate, metal substrate, isolated boron cluster, respectively, n is the number of boron clusters. We choose three metal substrates to demonstrate that the cohesive energy of these magnetic boron clusters on metal substrates is higher than those stable boron clusters reported previously, indicating that it is possible to synthesize these magnetic boron clusters on the proper substrates experimentally.

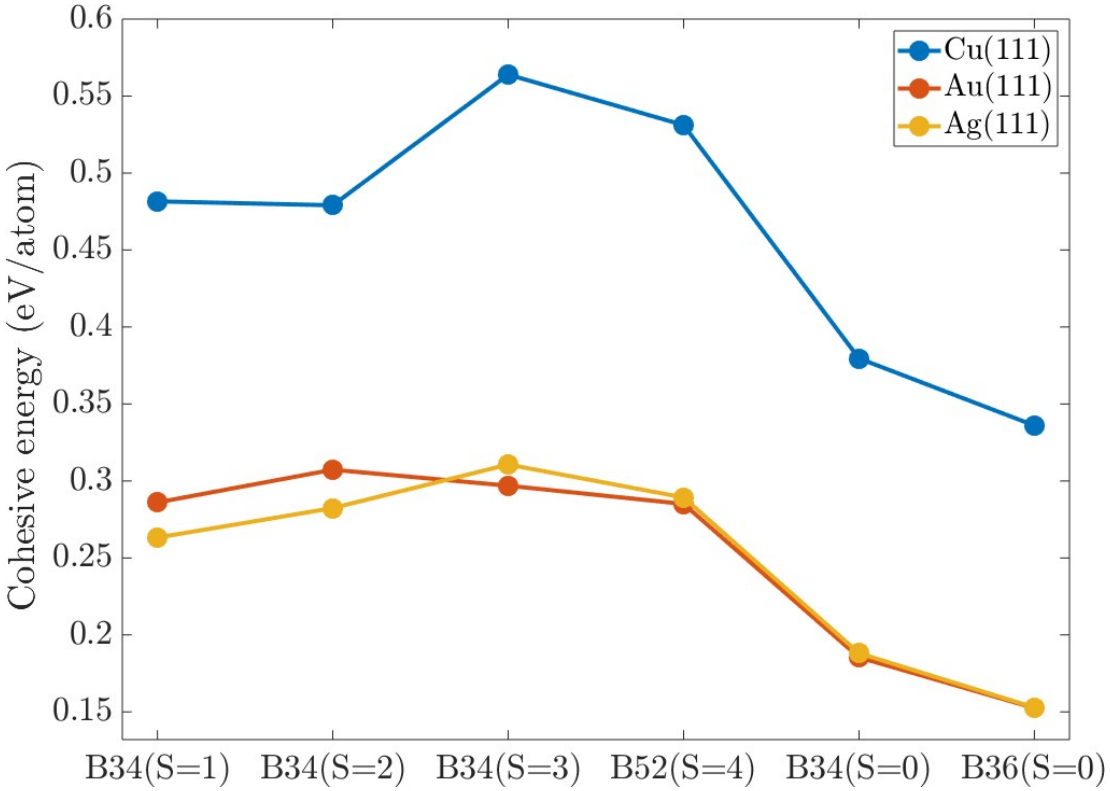

Figure S2. The cohesive energy of boron clusters at Cu(111), Au(111), Ag(111) metal substrates, where B34(S=1,2,3,4) clusters are predicted in this article and the B34(S=0), B36(S=0) clusters are the previous works.[1-2]

For boron monolayers, as listed in Table S2, we selected several monolayers from Zeng's[3] and Boldyrev's[4] work as examples for the comparison between the predicted magnetic boron monolayers and the proposed boron monolayers.

Table S2. Computed cohesive energy per atom of boron monolayers.

Boron sheet	E_c (eV/atom)
α[3]	5.990
χ_3[3]	5.919
χ_4[3]	5.907
2D-B_6[4]	5.762
B_{34}-triangular (Fig. 4a)	5.741
B_{34}- hexagonal (a) (Fig. 5a)	5.679
B_{34}- hexagonal (b) (Fig. 5b)	5.602
MS-boron (inset of Fig. 7a)	5.762

Calculation Details of $E_{majority}$ and $E_{minority}$

For the predicted $\alpha - B_{34}$ cluster, there are $34 \times 3 = 102$ valence electrons with six unpaired electrons at ground state, based on the DFT calculations. Then the majority spin state has $102 \div 2 + 3 = 54$ electrons while the minority spin state has $102 \div 2 - 3 = 48$ electrons, here $E_{majority}$ / $E_{minority}$ is defined by the mean energy levels

of the 49-th to 54-th energy level at the majority/minority spin state, respectively. For a nonmagnetic B_{34} cluster, the $E_{majority}$ is equal to $E_{minority,}$ in Fig. 3b, there is an apparent gap between the $E_{majority}$ and $E_{minority}$ during the AIMD simulation at room temperature, indicating the robustness of ferromagnetism induced from the $\alpha - B_{34}$ cluster.

Spatial Spin Distribution for Two Configurations in Fig. 3c.

When B atom is move from the position of the center to the corner. We have carefully checked the non-magnetic cluster in Figure 3c, and found that $E_{non\text{-}magnetic\_state}$-$E_{magnetic\_state}$= -2.35 meV (where $E_{non\text{-}magnetic\_state}$ is the total energy at non-magnetic state while $E_{magnetic\_state}$ is the total energy at magnetic state), confirming that the non-magnetic ground state due to 2.35 meV energy difference. Setting the magnetic state by fixing the number of spin majority/ minority electrons, we may find that the movement of B movement (red one in Figure. 3c) will not remarkably affect the spin charge distribution of the edges at upper right. The disappearance of magnetism might be caused by the symmetry broken of the $\alpha - B_{34}$ cluster, which makes the electron configuration with spin polarization become unstable. Below we will demonstrate the spatial spin distribution for the two configurations in Fig. 3c. Note that the upper right parts of the two configurations have similar spin distribution, however, the ground state of (b) B_{34} (non-magnetic) configuration exhibit non-magnetic characteristics, while the (a) B_{34} (magnetic) configuration is ferromagnetic at ground state.

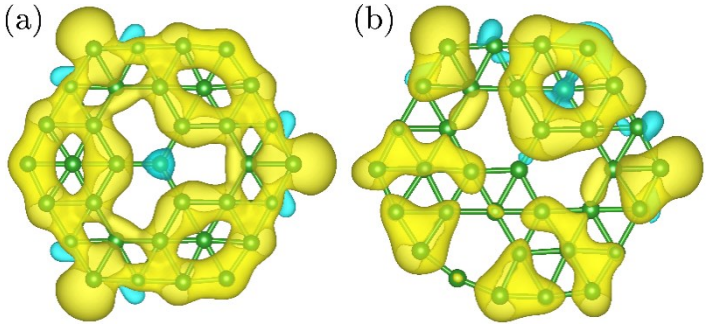

Figure S3. The spin charge distribution of (a) the magnetic B_{34} cluster and (b) the non-magnetic B_{34} clusters. The yellow/blue part denotes the majority/minority spin charge density.

Dynamic Stability Check

To check the dynamic stability of the predicted structures, we have calculated the phonon dispersion and *ab initio* molecular dynamics (AIMD) simulation to demonstrate the stability of these predicted magnetic monolayers. Due to the expensive computational cost, we have calculated the phonon frequency for the small system. The phonon dispersion was calculated by Phonopy code[6] using $3 \times 3 \times 1$ supercell. The phonon dispersion of these proposed structures are shown below. We perform 5000 steps (5 ps) of AIMD, and the simulation results show that the proposed boron monolayers will be stable at 300K.

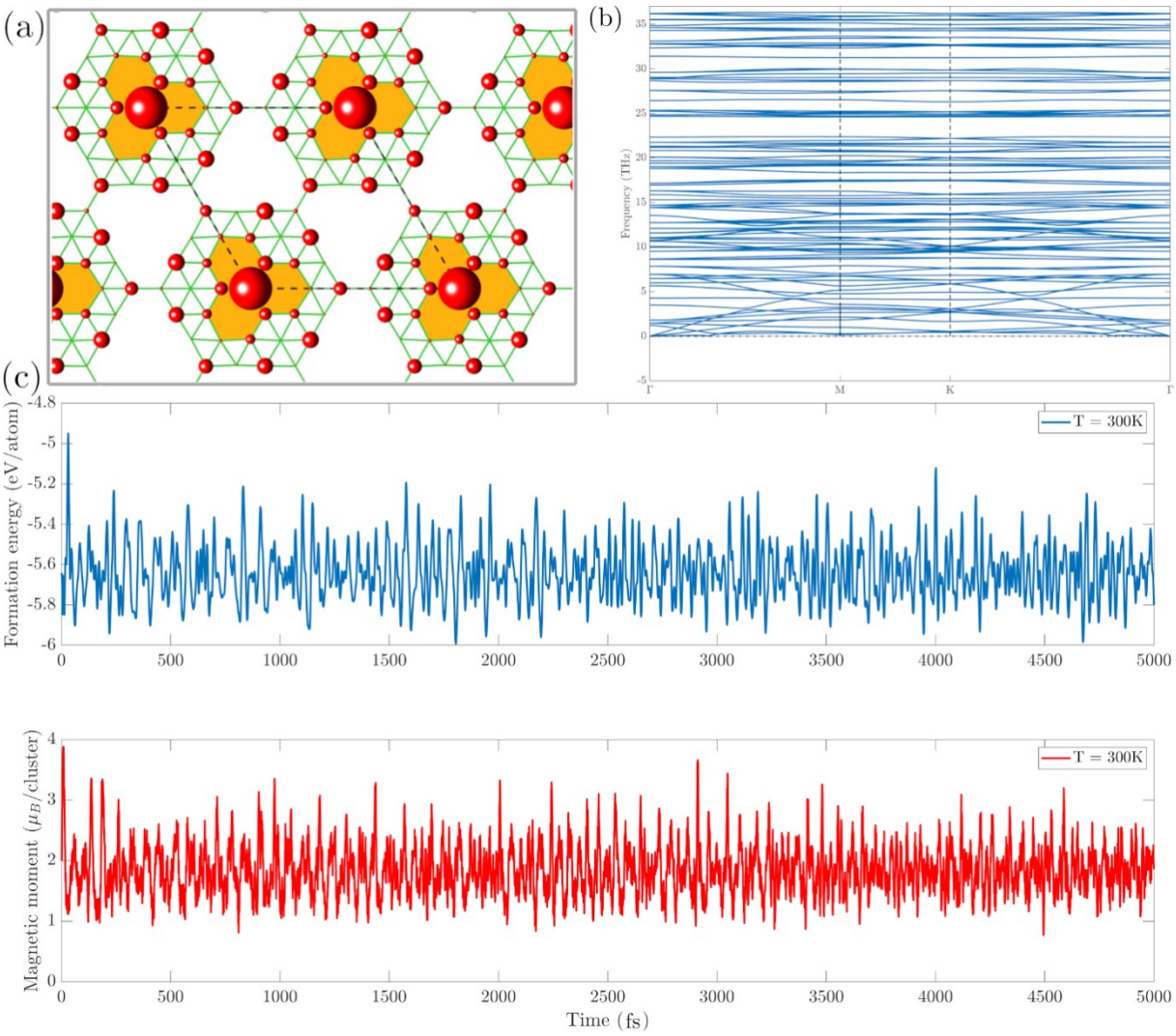

Figure S4. (a) In triangular lattice, the assembled boron monolayer with the rate of type-I at 0. (b) The calculated phonon dispersion curves along the G–M–X–G path for the ferromagnetic boron monolayer. (c) The calculated fluctuations of the temperature and total magnetic moment varies with the simulation time step at 300K. (Correspondent to Fig. 4a in the manuscript.)

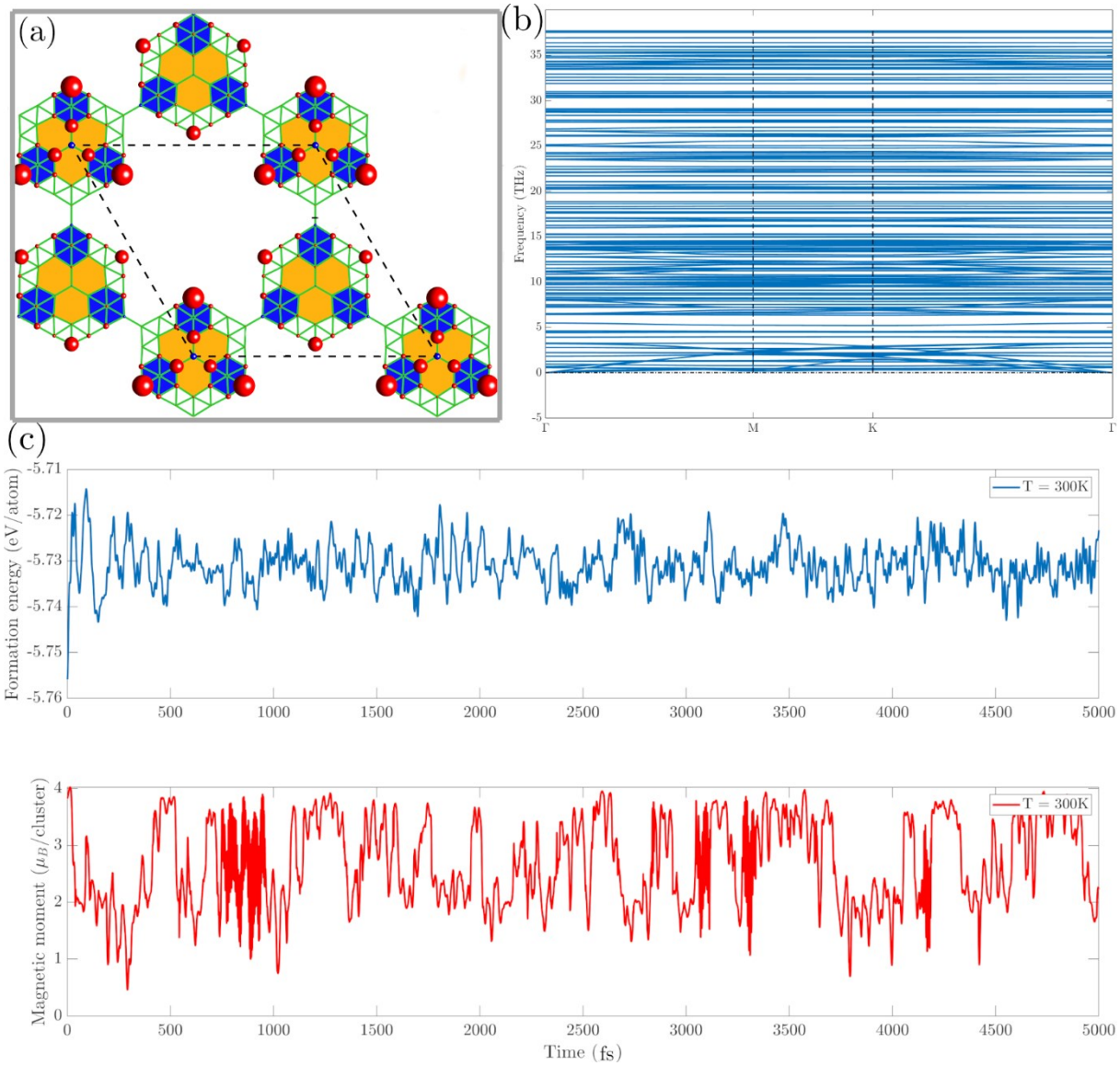

Figure S5. (a) In hexagonal lattice, the assembled boron monolayer with the rate of type-I at 0. (b) The calculated phonon dispersion curves along the G–M–X–G path for the ferromagnetic boron monolayer. (c) The calculated fluctuations of the temperature and total magnetic moment varies with the simulation time step at 300K. (Correspondent to the Fig. 5a in the manuscript.)

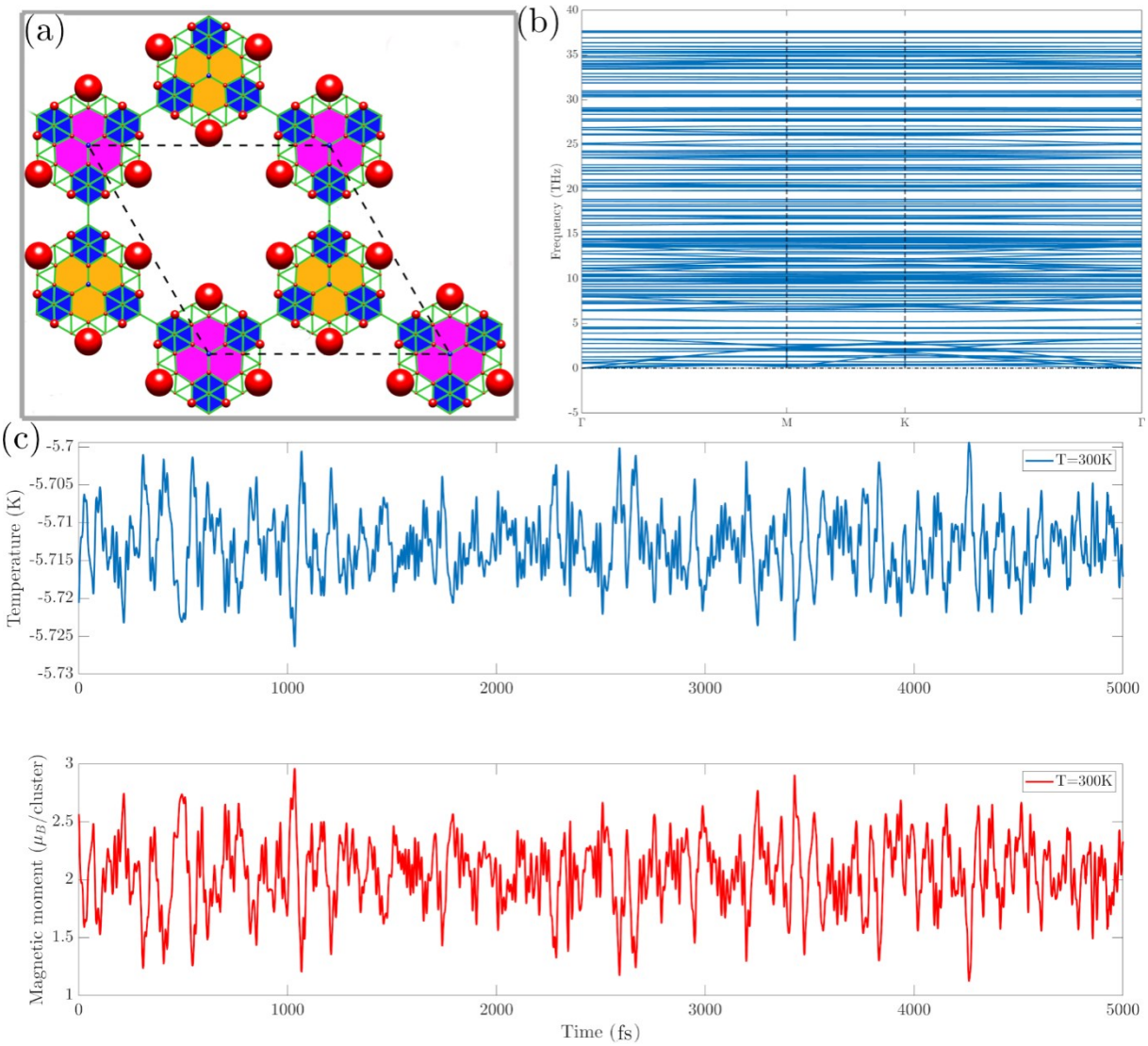

Figure S6. (a) In hexagonal lattice, the assembled boron monolayer with the rate of type-I at 1/2. (b) The calculated phonon dispersion curves along the G–M–X–G path for the ferromagnetic boron monolayer. (c) The calculated fluctuations of the temperature and total magnetic moment varies with the simulation time step at 300K. (Correspondent to the Fig. 5b in the manuscript.)

There are too many atoms in the unit cell of structure shown in Fig. 3b, and we cannot afford the computational cost of phonon dispersion calculations. Note that the AIMD calculation can also show the dynamic stability of the structure.

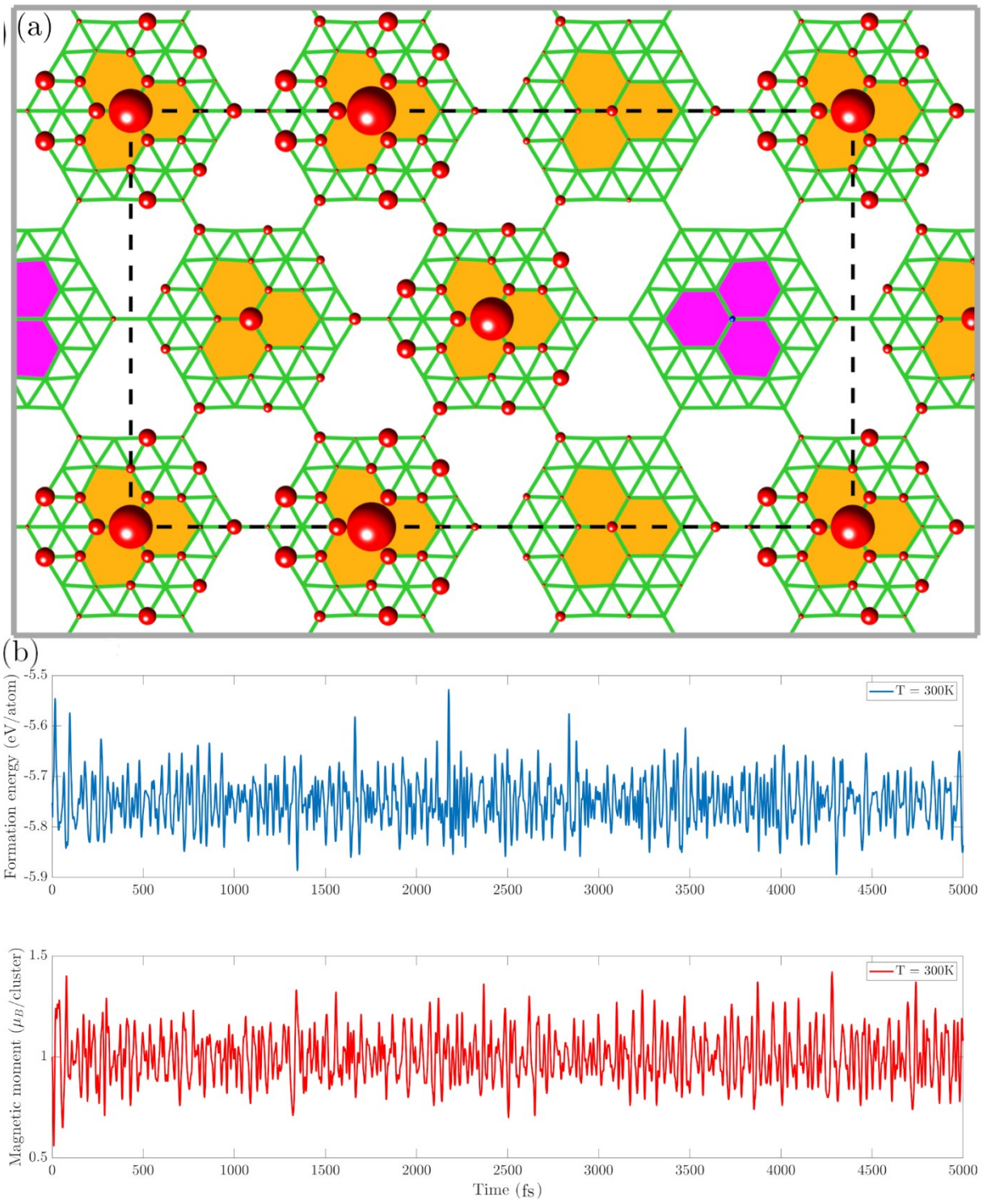

Figure S7. (a) In triangular lattice, the assembled boron monolayers with the rate of type-I at 1/6. (b) The calculated fluctuations of the temperature and total magnetic moment varies with the simulation time step at 300K. (Correspondent to the Fig. 4b in the article.)

Band Gap and Magnetic Moment at Finite Temperature

In general, Monte Carlo (MC) simulation through the random spin flipping is performed to describe the

evolution of magnetic moments in transition metal compounds, where the atomic displacements have less effect on the local magnetic moment from *d* electrons. However, *p* electrons is dominant to these predicted magnetic monolayers and the delocalized electrons may be the principal factor of the ferromagnetism. Furthermore, the magnetic phase transition may be attributed to the atomic vibration rather than the spin flipping of *p* electrons. In each temperature, the boron atoms will vibrate due to the effect of ambient temperature, which will cause the change of electronic structures. If the temperature of MD simulations is high enough, dramatic atomic vibrations will induce the magnetic-nonmagnetic phase transition. Note that the DFT calculations can tell us the magnetic moment and band gap in each step of AMID, therefore, we perform 10000 steps (10 ps) of AIMD, the mean magnetic moment is calculated by the time average of the last 1000 steps. Similarly, we estimate the average band gap based on AIMD with given temperature, which is the result of the atomic deviation. Furthermore, the non-self-consistent full random-phase approximation (RPA) formalism [5] has been proposed to evaluate the band gap at finite temperature in a relatively accurate level. However, we just adopt a relative convenient method to estimate the band gap with less computational expense.

Reference

[1] X. Sun, X. Liu, J. Yin, J. Yu, Y. Li, Y. Hang, X. Zhou, M. Yu, J. Li, G. Tai and W. Guo, *Adv. Funct. Mater.* 2017, **27**, 1603300.

[2] Q. Chen, W.-L. Li, X.-Y. Zhao, H.-R. Li, L.-Y. Feng, H.-J. Zhai, S.-D. Li and L.-S. Wang, *Eur. J. Inorg. Chem.*, 2017: 4546-4551.

[3] X. Wu, J. Dai, Y. Zhao, Z. Zhuo, J. Yang and X. C. Zeng, ACS Nano, 2012, 6, 7443–7453.

[4] N. V. Tkachenko, D. Steglenko, N. Fedik, N. M. Boldyreva, R. M. Minyaev, V. I. Minkin and A. I. Boldyrev, *Phys. Chem. Chem. Phys.***,** 2019, **21**, 19764–19771.

[5] A. Schenk, *J. Appl. Phys.*, 1998, **84**, 3684.

[6] A. Togo, F. Oba and I. Tanaka, *Phys. Rev. B: Condens. Matter Mater. Phys.*, 2008, **78**, 134106.